A comparative study between the addition of nano and micro-particles of Co_3O_4 on the electrical and microstructural properties of a ceramic system based on SnO_2

M.I. Miranda-López[a], M.B. Hernández[b], B.S. Vera-Barrios[c], A. Toxqui-Teran[d], and J.A. Aguilar-Martínez[a,*]

[a]*Universidad Autónoma de Nuevo León, Facultad de Ingeniería Mecánica y Eléctrica, Centro de Investigación e Innovación en Ingeniería Aeronáutica, Carretera a Salinas Victoria km. 2.3, 66600, Apodaca, N.L., México.*

[b]*Tecnológico de Monterrey, Escuela de Ingeniería y Ciencias, Av. Eugenio Garza Sada 2501, 64849, Monterrey, N.L., México.*

[c]*Universidad Nacional de Moquegua; Facultad de Ingeniería de Minas, Calle Ancash S/N, Moquegua, Perú.*

[d]*Centro de Investigación en Materiales Avanzados, S.C. Alianza Norte No. 202, Parque de Investigación e Innovación Tecnológica, Carretera Aeropuerto km. 10, 66600, Apodaca, N.L., México.*

[*]*e-mail: josue.aguilar74@gmail.com; josue.aguilarmrt@uanl.edu.mx*

Received 11 July 2019; accepted 17 September 2019

A comparative study between the addition of Co_3O_4 micro-particles and nano-particles as a densifying dopant of a SnO_2 based varistor system was conducted. The ceramic composition was (99.9-X) %SnO_2-X % Co_3O_4-0.05 %Cr_2O_3-0.05 %Nb_2O_5 where X = 0, 0.5, 1.0, 2.0 and 4.0 mol%. Two particle sizes of Co_3O_4 were used (~ 5 μm and ~ 50 nm). The addition of 0.5 mol% of Co_3O_4 nano-particles promoted an increase of grain size of the sintered samples up to 7.9 μm, that is, the maximum value among all variations. Characterization techniques such as TGA, DTA, XRD, and Rietveld analysis revealed a decrease of 16°C in the formation temperature of Co_2SnO_4 as well as an increase of 2.6 wt% in the amount of such phase with the use of 4.0 mol% of Co_3O_4 nano-particles in comparison with micro-particles. Statistical analysis indicated that the addition of nano-particles of Co_3O_4 yielded better repeatability on the densification of ceramic samples. Also, residual porosity was decreased. Electrical breakdown and non-linear coefficient values correspond to a non-ohmic behavior with a potential application for manufacturing high voltage varistors. The findings of this work can be used as a reference for conducting a later study to improve the electrical properties or even to lower the sintering temperature.

Keywords: Electrical properties; varistors; sintering; grain boundaries; breakdown voltage.

PACS: 81.20.Ev; 61.05.cp; 84.32.Ff.

DOI: https://doi.org/10.31349/RevMexFis.66.47

1. Introduction

The on-going development of the electronics industry requires that the integrity of equipment that is sensitive to abrupt voltage changes be safe. A practical solution for that problem in home appliances and industrial equipment is the use of surge absorber devices, such as varistors. It is widely known that metal oxide varistors (MOVs) are advanced ceramics whose resistance is voltage-dependent. When an electric potential difference is applied to a MOV, its electrical behavior can change from a resistive-state into a conductor-state at the same time that the voltage reaches a specific value (known as the breakdown voltage). This voltage-dependence is also called non-linear electrical behavior [1]. Since MOVs are commonly used in parallel with electrical circuits, their non-linear behavior enables the clamping down of surges if the nominal voltage is under the breakdown voltage and thus offering a safe way out when the said limit is overcome. In recent years, MOVs have been used to fabricate sophisticated surge arrester devices or even as current sensors [2].

The formation of potential barriers is required to enable the non-linear properties in ceramic materials [3], therefore, it becomes imperative to obtain a highly dense material. The grain size, the constituent phases, and the intrinsic grain conductivity also play an important role [1]. Varistor systems based on SnO_2 have been widely studied as an alternative for ZnO. The main advantages of the use of SnO_2 over ZnO are: higher resistance to degradation and single-phase structure [4]. The microstructure of sintered pure SnO_2 exhibits high porosity and grains linked by the necking effect due to an evaporation-condensation mechanism [5]. Density can be increased by the creation of oxygen vacancies which promote the mass transport from inside the grains to the grain boundaries [6]. To achieve the aforementioned task, several researches have used densifying agents such as CaO [7] , CuO [8], ZnO [9], and Co_3O_4 [10], to name just a few. The accumulation of defects at the grain boundaries due to the dopant inclusion leads to a charge concentration and thus the formation of potential barriers [11].

During the last few years, a new branch of electroceramics that involves nanotechnology has emerged [12,13]. This not only enables the possibility of fabricating more complex

and advanced devices, but it also improves the features of the actual materials and their processing. In particular, for SnO_2 based varistors, a growing body of literature has been published reporting results of nanostructured precursors used to enhance densification [12-14]. This work aims to evaluate and compare the performance of the micro and nanoparticles of Co_3O_4 as a densifier dopant. Microstructural development, as well as the non-ohmic electrical properties, are also discussed to establish a correlation with the particle size.

2. Experimental Procedure

In this work, SnO_2, Co_3O_4 (50 nm and 5 μm particle size), Cr_2O_3, and Nb_2O_5 analytical grade starting materials (from Aldrich) were used. The molar composition of the investigated system was (99.9-X)% SnO_2 - X% Co_3O_4 - 0.05% Cr_2O_3 - 0.05% Nb_2O_5, where X = 0.0, 0.5, 1.0, 2.0 and 4.0%. A high energy planetary ball mill (Pulverisette 7) was used to obtain a homogeneous powder mixture. A polypropylene vial of 50 cm^3 inner volume was filled with the starting oxides, 15 ml of distilled water, and 180 agate balls of 5 mm diameter to obtain a slurry. Milling parameters were 300 rpm for 60 min. The planetary mill allows the use of a reversing function in such a way that the direction of rotation can be changed after a chosen period until the full cycle is completed. Therefore, this reversing function was used to enhance the homogeneity of the powder mixture.

After milling, the obtained slurry was dried at 80°C for 4 h. The dried powders and 5% wt. of Polyvinyl alcohol, PVA, as a binder, were uniaxially pressed in the form of tablets (10.0 mm in diameter and 1.2 mm in thickness) at 176 MPa.

The tablets were sintered in an ambient atmosphere at 1350°C for 1 h with a heating and cooling rate of 6°C/min in a tube furnace (Nabertherm RHTC 80-230/15). Silver electrodes (SPI flash-dry silver paint) were applied on both faces of the ceramic sintered tablets before electrical characterization. Current-voltage measurements were taken using a High Voltage Measure Unit (Keithley 2657A). The nonlinear coefficient α can be calculated using the relation:

$$\alpha = \frac{\log(J_2/J_1)}{\log(E_2/E_1)} \tag{1}$$

where E_1 and E_2 are the applied electric fields related to the current densities $J_1 = 1\,\mathrm{mAcm}^{-2}$ and $J_2 = 10\,\mathrm{mAcm}^{-2}$, respectively. Breakdown voltage E_B is measured at $1\,\mathrm{mAcm}^{-1}$ while J and E are calculated using i/s and V/t, where i is the electric current, s is the area of the silver electrode, and t is the thickness of the tested sample.

Measurements to calculate the density of sintered samples were made using the Archimedes' method and compared to the theoretical density obtained from the rule of mixtures. X-ray diffraction technique (XRD; PANalytical Empyrean model) was used to identify phases of samples under the following conditions: CuKα radiation ($\lambda = 1.5406$ Å) operated

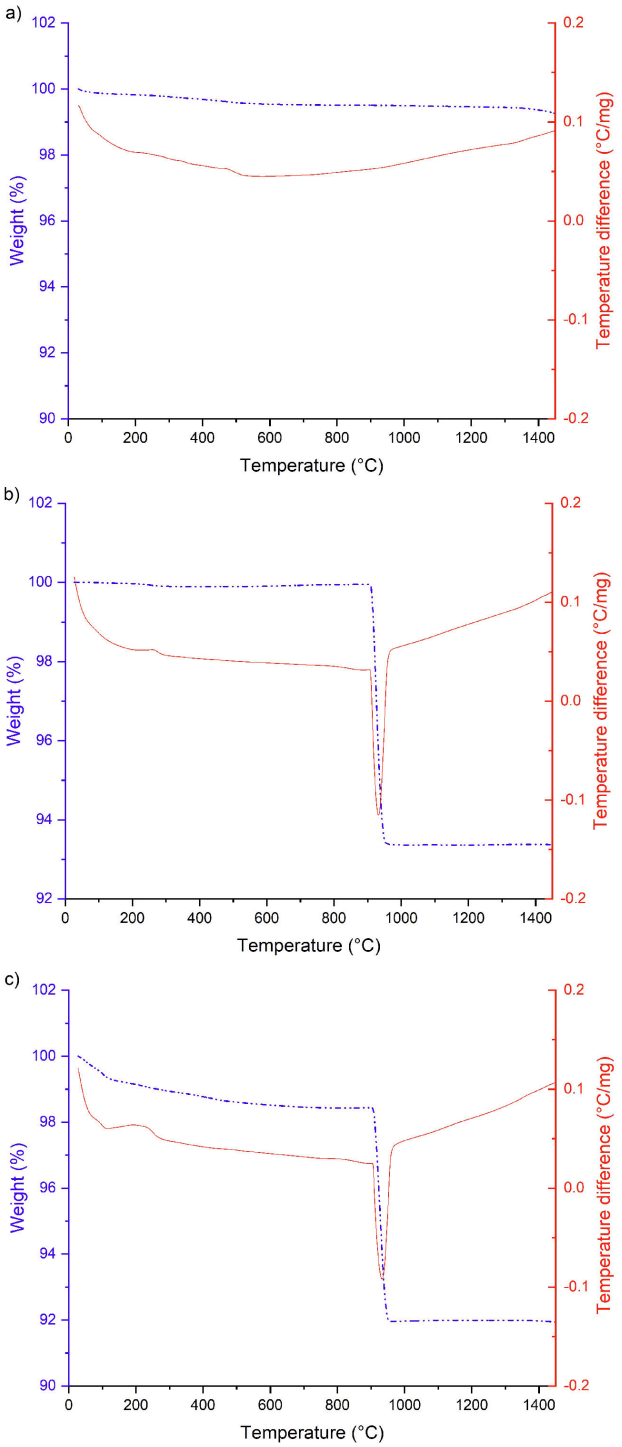

FIGURE 1. Thermograms from a) pure SnO2, b) Co_3O_4 micro-particles, and c) Co_3O_4 nano-particles.

at 45 kV, 40 mA and a PIXel 1D detector in Bragg-Brentano geometry. The scans were performed in the 2θ range from 10 to 80° with a step scan of 0.016° and 10 s per step in a continuous mode. Grain size and morphology of the samples were characterized by scanning electron microscopy (SEM; model Nova Nano SEM 200, FEI). The mean grain size was calculated from SEM micrographs with the aid of an image

analysis software (Image-Pro Plus), according to the ASTM-E112 standard procedure.

3. Results and discussion

It has been previously reported by the authors that tin oxide exhibits good thermal stability in the temperature range from ambient up to 1450°C, where the sintering process of the reference sample takes place. The minimum weight loss observed (Fig. 1a) is a consequence of the evaporation of chemical water [15].

Thermograms corresponding to micro and nano-particles of Co_3O_4 (Figs. 1b and 1c) show two similar processes. For the micro-particle powder sample, there is an exothermic reaction between 50 and 250°C caused by the evaporation of water absorbed by the compound, shown in Fig. 1b. The weight of the sample decreased by 0.06% during this process. Subsequently, the presence of an endothermic peak at 933°C in the DTA curve and a weight loss of 6.57% is related to the formation of CoO from Co_3O_4, according to the following reaction:

$$2C\ o_3O_4 \xrightarrow{933^\circ C} 6Co\ O + \uparrow O_2 \qquad (2)$$

On the other hand, the thermogram corresponding to the nano-particle powder of Co_3O_4 (Fig. 1c), shows a weight loss of 1.57%, due to the evaporation of water at a lower temperature than that from the micro particles. The formation of CoO is also carried out at a temperature of 933°C, according to Eq. (2). A reduction in weight of 6.47% takes place at this temperature.

Thermograms from samples doped with micro and nano-particles of Co_3O_4 were also obtained (Figs. 2a and 2b) and compared. In general, both systems exhibit similar behavior: approximately 150°C, an exothermic process caused by the evaporation of water in the mixture is observed. Subsequently, an endothermic peak related to the reduction of

Co_3O_4 to CoO Eq. (2), and its interaction with SnO_2 encourages the *in-situ* formation of the spinel phase Co_2SnO_4, which occurs at 945°C when using micro-particles of Co_3O_4 and at 929°C with nano-particles. This endothermic peak is not observed in the samples with 0.5%. However, as the concentration of Co_3O_4 increases, the intensity increases until reaching its maximum value for the sample with a concentration of 4.0%. The following equation shows the process:

$$2Co\ O + Sn\ O_2 \rightarrow\ Co_2Sn\ O_4. \qquad (3)$$

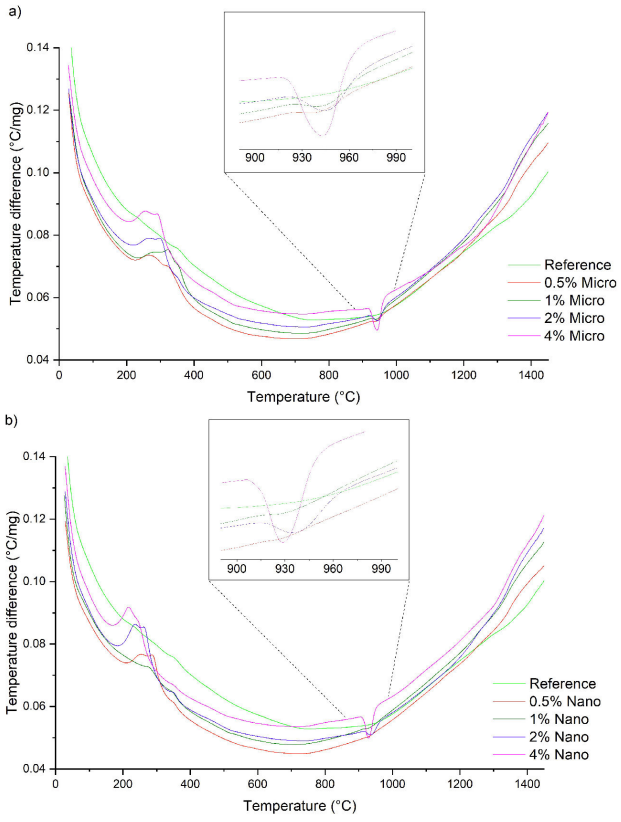

FIGURE 2. Thermograms from ceramic samples doped with a) Co_3O_4 micro-particles, and b) Co_3O_4 nano-particles.

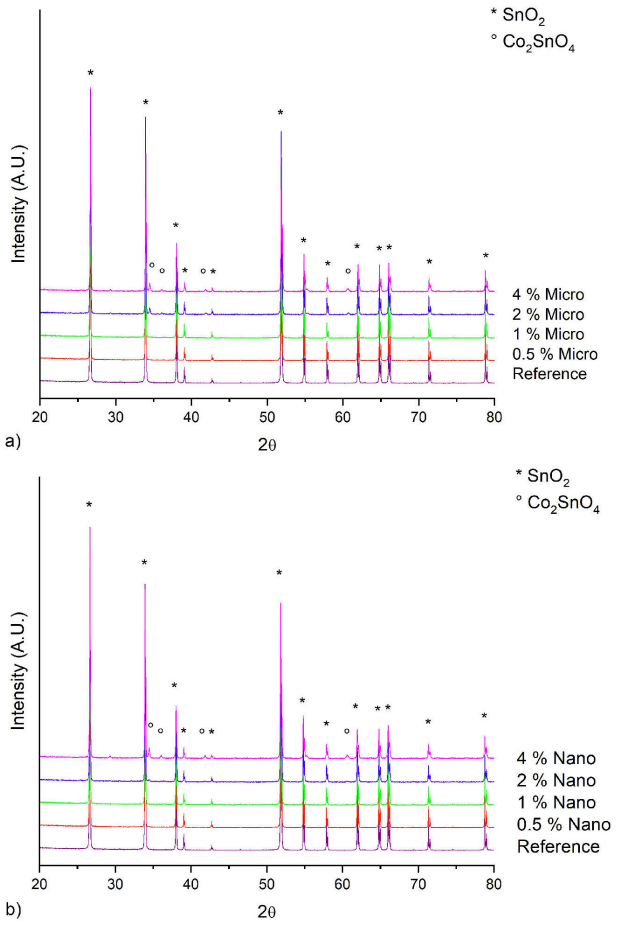

FIGURE 3. Diffraction patterns from samples for reference sample and all compositions doped with a) Co_3O_4 micro-particles, and b) Co_3O_4 nano-particles.

TABLE I. Weighted profile magnitude (R_{wp}), projected magnitude (R_{exp}), profile magnitude (R_P), optimum fit magnitude (χ^2), and lattice constant.

Sample	Phase	Lattice parameter (Å)				wt(%)	R_{wp}(%)	R_{exp}(%)	R_p(%)	χ^2
	Present	a	b	c	$\alpha=\beta=\gamma$					
Reference	SnO2	4.736	4.736	3.186	90	100	6.97	12.71	17.08	2.402
0.5% Co_3O_4 micro	SnO_2	4.737	4.737	3.186	90	100	7.50	16.06	21.97	2.930
0.5% Co_3O_4 nano	SnO_2	4.737	4.737	3.186	90	100	7.37	16.04	21.73	2.950
1% Co_3O_4 micro	SnO_2	4.737	4.737	3.186	90	100	7.16	16.05	22.19	3.100
1% Co_3O_4 nano	SnO2	4.736	4.736	3.186	90	100	6.93	13.72	19.03	2.747
2% Co_3O_4 micro	SnO2	4.737	4.737	3.186	90	97.4	6.21	14.84	19.53	3.145
	Co_2SnO_4	8.644	8.644	8.644	90	2.6				
2% Co_3O_4 nano	SnO_2	4.736	4.736	3.186	90	96.3	6.52	13.99	18.67	2.623
	Co_2SnO_4	8.644	8.644	8.644	90	3.7				
4% Co_3O_4 micro	SnO_2	4.737	4.737	3.186	90	91.9	5.88	10.88	15.40	2.618
	Co_2SnO_4	8.645	8.645	8.645	90	8.1				
4% Co_3O_4 nano	SnO_2	4.736	4.736	3.186	90	89.4	5.54	9.73	14.28	2.434
	Co_2SnO_4	8.642	8.642	8.642	90	10.6				

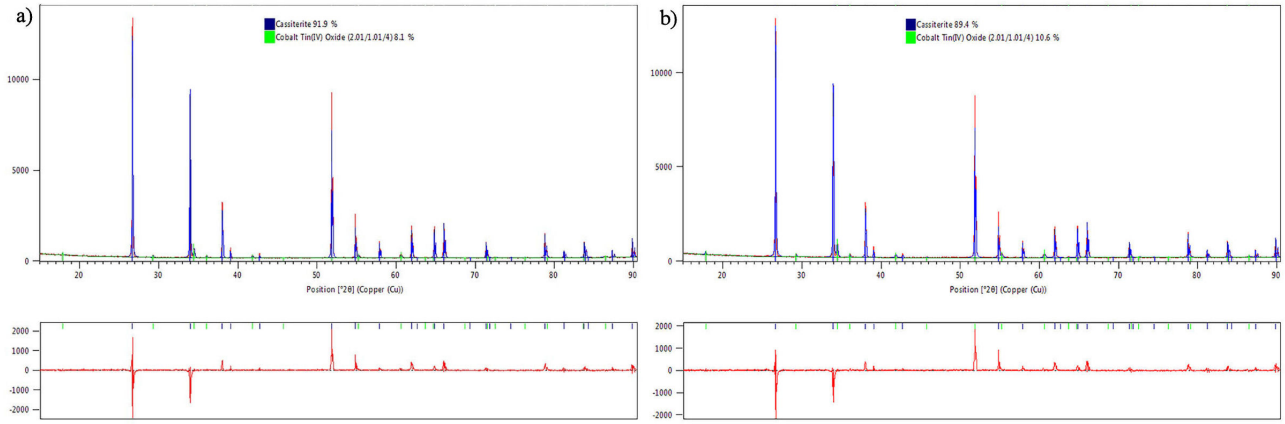

FIGURE 4. Profile refinement plot for samples with a) 4 mol% Co_3O_4 micro-particles, and b) 4 mol% Co_3O_4 nano-particles. Experimental data (red line) and calculated XRD pattern (blue line). The bottom plot shows the difference between experimental and calculated data, as well as the reflections of SnO_2 and Co_2SnO_4 (vertical lines).

Previous studies in the field [16,17] have presented results that are consistent with those obtained here regarding the formation of Co_2SnO_4 from the interaction between CoO and SnO_2. However, the temperature at which the Co_2SnO_4 phase is formed during the thermal process has a difference of 16 degrees when using nano-particles instead of micro-particles of Co_3O_4. The authors suggest that this difference is due to the higher surface area of the nano-particles. It is assumed that the small amount of Cr_2O_3 and Nb_2O_5 have a negligible effect such that they do not produce any impact on the thermal behavior of the samples.

Diffractograms from samples doped with micro and nano-particles are presented in Fig. 3. The peaks shown match the diffraction pattern of the tetragonal rutile type SnO_2 crystal structure (ICDD PDF 01-070-6995). Samples doped with 2.0 and 4.0 mol% of Co_3O_4 exhibit evidence of the spinel-type phase Co_2SnO_4 with a cubic crystalline structure. This is suggested by the pairing of the remaining peaks with the standard ICDD PDF 01-073-1617. The formation of this phase during sintering of cobalt oxide-doped varistors has been previously reported [10]. Additionally, this data supports the results from thermogravimetric studies where the reduction of Co_3O_4 to CoO, leads to the formation of Co_2SnO_4.

From the Rietveld refinement (Table I), it was possible to determine that an increase of Co_3O_4 content leads to an increase in the formation of the spinel phase. Figure 4 shows the observed, calculated, and difference plots for the samples with the higher content of Co_3O_4. Additionally, it was also possible to determine that the use of nano-particles enhances the formation of the Co_2SnO_4 spinel phase. This can be explained by relating the surface free energy of both of the

TABLE II. Median value of contraction (γ), theoretical density (ρ_t) quantified density (ρ), relative density (ρ_r), remaining porosity (P), nonlinearity coefficient (α), electric field (E_B) and average grain size of sintered specimens.

Sample	γ (%)	ρ_t (gcm^3)	ρ (gcm^3)	ρ_{tr} (%)	P (%)	α	E_B (V/cm)	Grain size (μm)
Reference	6.0	6.95	6.64	95.54	4.46			
0.5% Co_2SnO_4 micro	14.1	6.94	6.80	97.98	2.02	5	2536	6.7
0.5% Co_2SnO_4 nano	14.0	6.94	6.80	97.98	2.02	2	1162	7.9
1% Co_2SnO_4 micro	14.5	6.94	6.77	97.55	2.45	2	1076	7.9
1% Co_2SnO_4 nano	14.8	6.94	6.79	97.84	2.16	3	1219	7.9
2% Co_2SnO_4 micro	14.2	6.93	6.74	97.26	2.74	6	2645	6.7
2% Co_2SnO_4 nano	14.1	6.93	6.82	98.41	1.59	2	1647	5.6
4% Co_2SnO_4 micro	13.4	6.91	6.64	96.09	3.91	7	3758	5.6
4% Co_2SnO_4 nano	14.0	6.91	6.72	97.25	2.75	3	2386	4.7

*Theoretical density obtained from the rule of mixtures

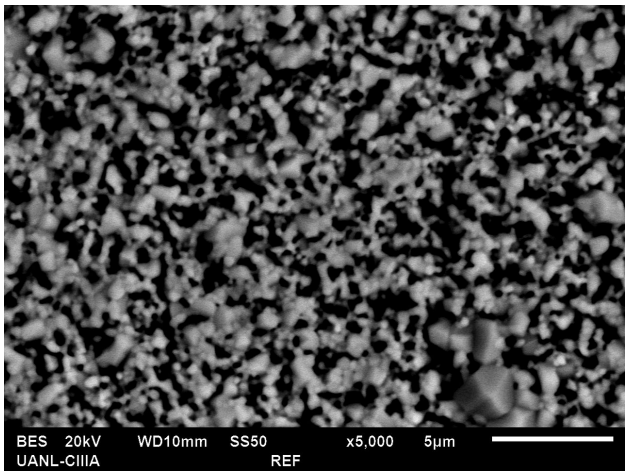

FIGURE 5. Micrograph from pure SnO_2 sample.

Co_3O_4 particle sizes used. A smaller particle size is related to higher superficial energy [18]. Based on the previous statement, it should be expected that shown reactions in Eqs. (2) and (3) are more spontaneous with the use of nano-particles rather than micro-particles, due to the high tendency of the nano-particles surface to bind their disjointed bonds.

Equations (2) and (3) support the statement that any amount of Co_3O_4 will produce Co_2SnO_4 under the indicated conditions. However, the scope of the XRD technique does not allow the determination of the phases present within the samples in concentrations below 1.0 %. Therefore, the presence of the other oxides (Cr_2O_3 and Nb_2O_5) cannot be identified.

Figure 5 shows micrographs from the reference sample where only SnO_2 particles are present, and it can be seen that small joints have formed between the particles due to the diffusion of oxygen when the sample is subjected to high temperatures. The highly porous structure shown is expected since the diffusion is not active enough for pure SnO_2.

Micrographs from samples doped with micro and nano-particles of Co_3O_4 are shown in Fig. 6. Table II summarises, the grain size calculated from SEM images. From these results it can be established that doping with cobalt oxide, even in small concentrations of 0.5 mol% stimulates grain growth. Previous studies [19] have indicated that the densification process in SnO_2-based materials is carried out when ions of Sn^{4+} are replaced by Co^{2+} in the crystal lattice during the sintering stage. The charge compensation, due to the difference in the valences of Sn and Co produces oxygen vacancies giving rise to its diffusion and therefore to grain growth. This mechanism can be described by the following expressions:

$$\text{Co O} \xrightarrow{\text{SnO}_2} \text{Co}''\text{Sn} + \text{V}\ddot{\text{o}} + \text{O}_O^X \tag{4}$$

$$\text{Co O} \xrightarrow{\text{SnO}_2} \text{Co}''\text{Sn} + \text{V}\dot{\text{o}} + \frac{1}{2}\text{O}_2 \uparrow . \tag{5}$$

In the varistors that were doped with micro-particles of Co_3O_4, a very slight increase in the average grain size is observed when going from 0.5 to 1.0 mol% (Figs. 6a and 6c). Later, a decrease of grain size is observed when 2.0 and 4.0 mol% are used, down to a value of 5.6 μm (Figs. 6e and 6g). On the other hand, when Co_3O_4 nano-particles were added, the average grain size was kept constant at a value of 7.9 μm for concentrations of 0.5 and 1.0% (Figs. 6b and 6d). As the nano-particle content increases, a decrease in grain size was observed for samples with concentrations of 2.0 and 4.0 mol%.

SEM images show that porosity in the samples is almost negligible, even with the lowest concentration of Co_3O_4. This feature is desirable in a varistor since porosity has a detrimental effect on electrical properties. Differences in grain size are noticeable and the non-homogeneous morphology in the grains is evident. Particularly, samples with 2.0 and 4.0 mol% Co_3O_4 have a visibly smaller grain type with sharp edges associated with the Co_2SnO_4 phase. The latter is confirmed by the elemental analysis performed on the sample doped with

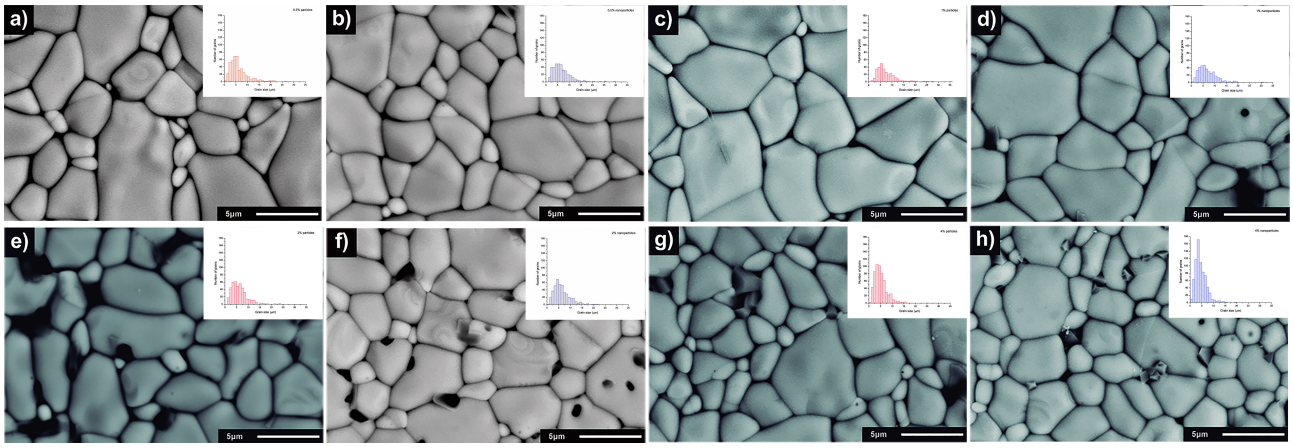

FIGURE 6. Micrographs from samples doped with a) 0.5, c) 1, e) 2, g) 4 mol% Co_3O_4 micro-particles, and b) 0.5, d) 1, f) 2, h) 4 mol% Co_3O_4 nano-particles.

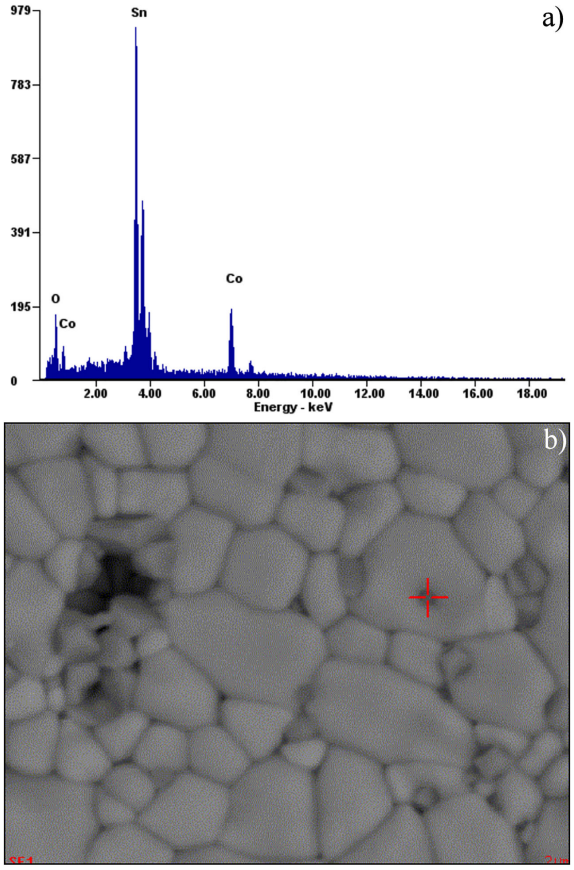

FIGURE 7. a) Micrograph from sample with 4 mol% Co_3O_4 micro-particles; b) EDX spectra from region mark with (+) showing the presence of Co.

4.0 mol% Co_3O_4 micro-particles (Fig. 7), where it is revealed that its composition contains a considerable amount of Co. At a concentration of 2.0 mol%, it is easy to find Co_2SnO_4 inside some SnO_2 grains (Figs. 6e and 6f).

Another outcome from the micrographs is that as the amount of Co_3O_4 increases, so does the grain size of the Co_2SnO_4 phase, while it irregulary agglomerates at grain boundaries promoting pore formation. By comparing the use of micro and nano-particles of Co_3O_4, the formation of the Co_2SnO_4 phase is more evident in the sample doped with a concentration of 4.0 mol% using nano-particles. This difference is well observed in Figs. 5g and 5h, and results from the Rietveld refinement can support this claim. It is interesting to note that the formation of Co_2SnO_4 could be responsible for the abrupt decrease in the grain size of samples with 2.0 and 4.0% Co_3O_4.

Box plot graphs (Fig. 8) show the dispersion in density values from all the studied samples. The reference sample exhibits the lowest density value and widest dispersion, from

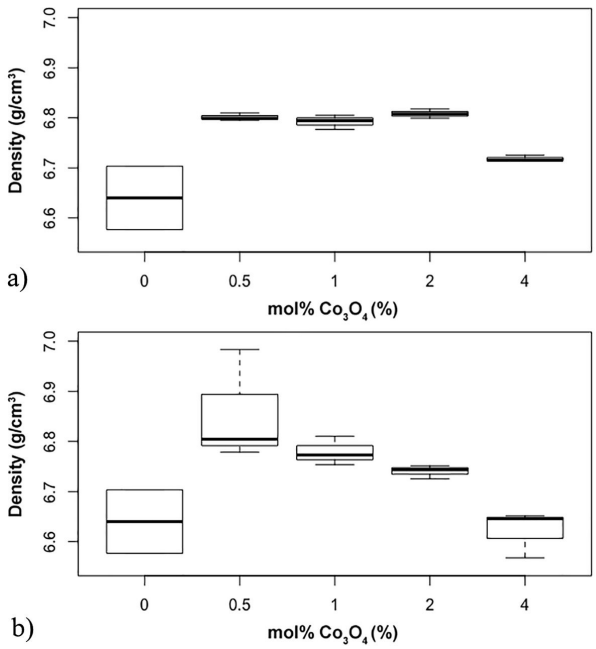

FIGURE 8. Density box plot from samples doped with a) Co_3O_4 nano-particles, and b) Co_3O_4 micro-particles.

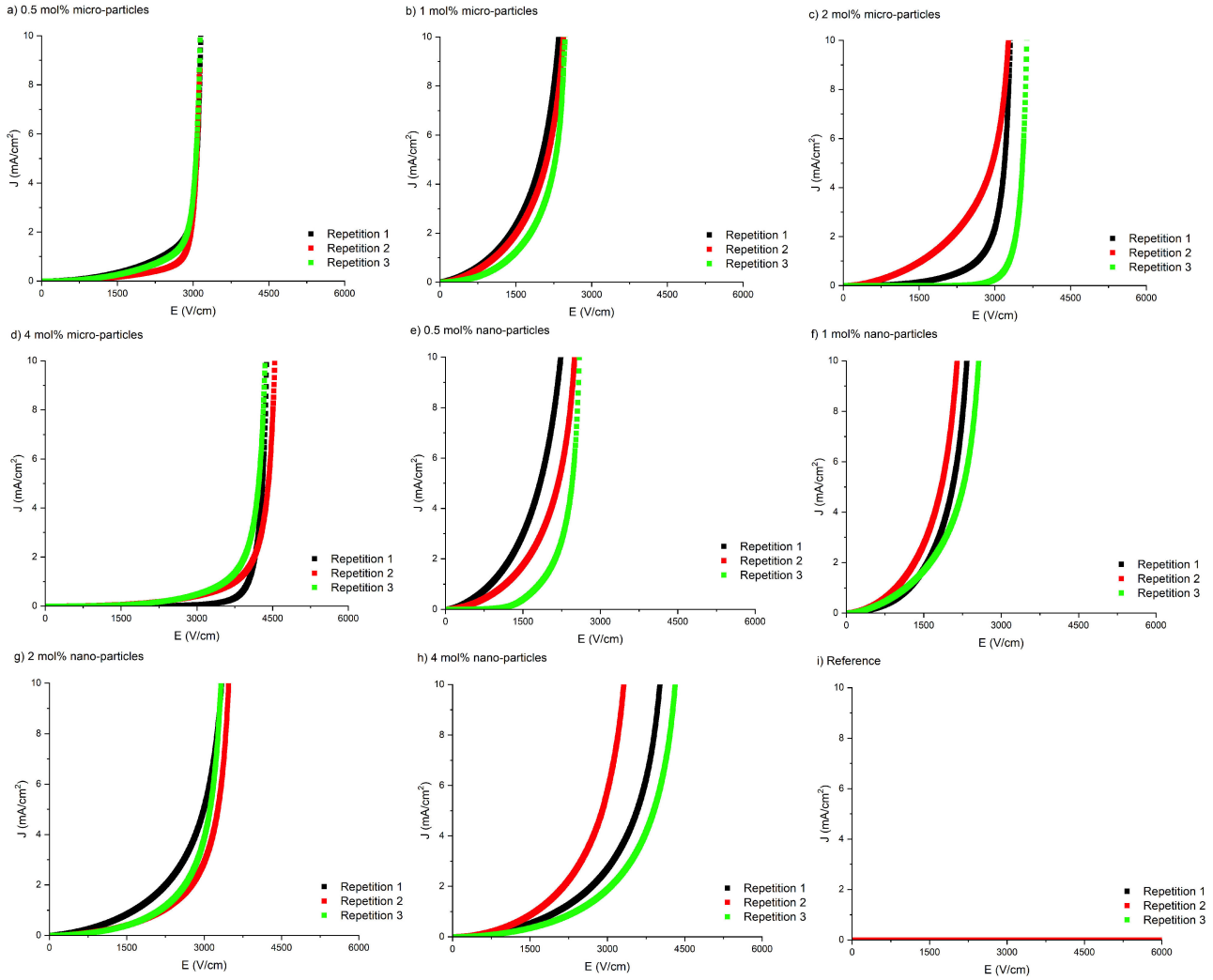

FIGURE 9. Electrical properties J vs. E from samples doped with a)- d) Co_3O_4 micro-particles; e)-h) Co_3O_4 nano-particles; i) reference sample, and their corresponding repetition.

6.58 $g cm^{-3}$ to 6.70 $g cm^{-3}$. The graph in Fig. 8a represents the density data obtained from samples doped with Co_3O_4 nano-particles. Narrower boxes were obtained, meaning that high repeatability in density was achieved. For samples with 0.5, 1.0 and 2.0% mol concentrations, the median density values are 6.80, 6.79 and 6.82 $g cm^{-3}$, respectively. However, a decrease in density occurred for the sample with 4.0 mol% concentration, down to 6.72 $g cm^{-3}$.

On the contrary, when micro-particles of Co_3O_4 were used, the dispersion of the data was wider, as can be confirmed by the distance between the limits of the boxes with their respective median values (Fig. 8b). A slightly constant decrease in density is observed for samples with 0.5, 1.0, and 2.0% mol concentration whose values are 6.80, 6.77, and 6.74 g cm^{-3}, respectively. Once again, for samples with the highest concentration of 4 mol%, a decrease in density is evident, with a median value of 6.64 $g cm^{-3}$. There is a noticeable difference in the repeatability of density values for ceramic samples doped with micro and nano-particles, the latter producing the lowest dispersion.

Figure 9 presents the characteristic representation of J vs. E for all studied samples in which the non-linear behavior is obvious. A statistical analysis of the breakdown voltage and the non-linear coefficient is presented in Fig. 10.

For samples doped with 0.5 and 1.0% mol of Co_3O_4 nano-particles, the median value of the breakdown voltage remained constant around 1200 $V cm^{-1}$. Samples with the lowest concentration, which is 0.5 mol%, show good reproducibility around the aforementioned value. A considerably higher than normal Eb was recorded at 2980 $V cm^{-1}$.

A progressive increase in breakdown voltage value is notable for samples with concentrations of 2.0 and 4.0% with median values of 1,647 and 2,386 V cm^{-1}, respectively. For samples prepared with micro-particles of Co_3O_4, a different trend is observed. The lowest concentration of 0.5% of Co_3O_4 produces a median value of breakdown voltage of 2,536 V cm^{-1}. Later, a decrease is observed, followed by a constant increase going through 1076, 2645 and 3758 V cm^{-1}, for samples at concentrations of 1.0, 2.0 and 4.0%, respectively.

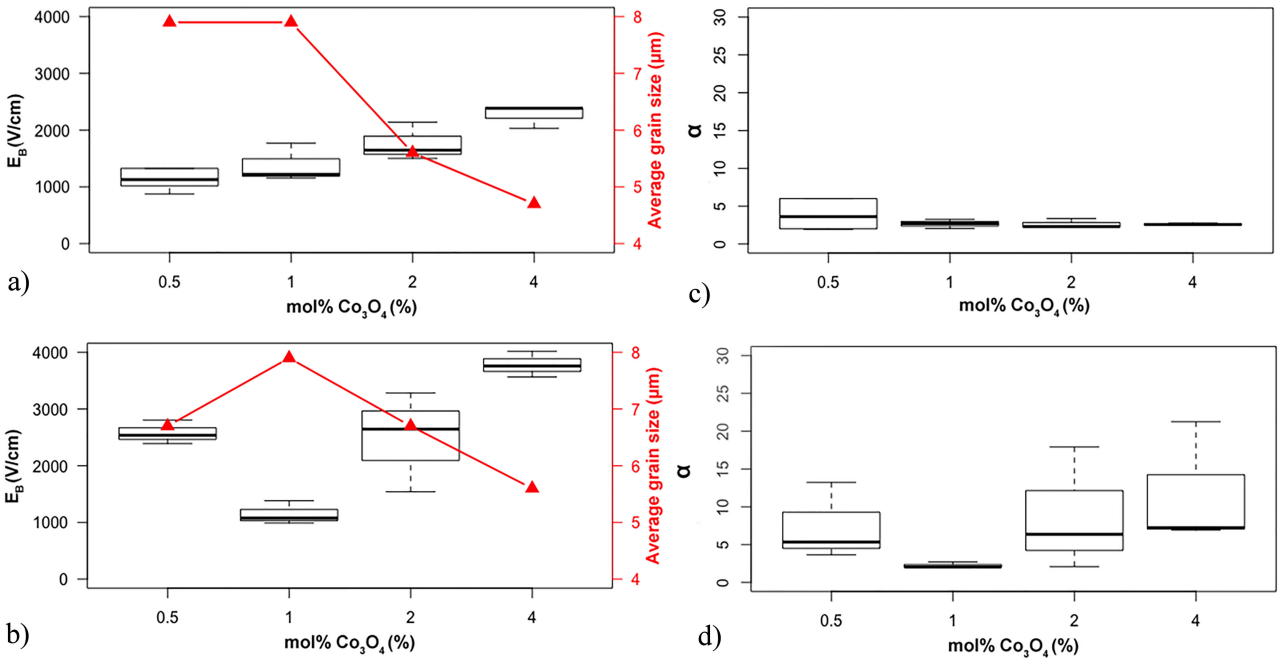

FIGURE 10. Breakdown electric field box plot from samples doped with a) Co_3O_4 nano-particles, and b) Co_3O_4 micro-particles. Non-linear coefficient box plot from samples doped with c) Co_3O_4 nano-particles, and d) Co_3O_4 micro-particles.

An interesting aspect to highlight is the fact that any increase or decrease in the mean values of breakdown voltage is consistent with the average grain size marked in red in the figures. This was an expected condition since the relationship between grain size and the value of the breakdown voltage is inversely proportional.

The α coefficient can be analyzed in the same way as the breakdown voltage, as shown in Figs. 10c and 10d. These figures represent the dispersion of the coefficients obtained for each of the concentrations and particle sizes.

The box that corresponds to the samples obtained with 0.5 mol% nano-particles of Co_3O_4 exhibits a median value of 3 and, as with the Eb analysis, there is an extreme value of 29 for one of the analyzed samples. For the concentrations of 1.0, 2.0 and 4.0 mol%, values are obtained with low dispersion (around 2).

The use of micro-particles of Co_3O_4 at a concentration of 0.5 mol% of Co_3O_4 enhances an increase of the α coefficient in comparison with the use of nano-particles, with a median value of 5, and a wide dispersion is obtained. Subsequently, with 1.0 mol%, the value of α decreases to 2 and low dispersion is observed. An increase of Co_3O_4 also causes a slight increase in the α coefficient, moving to values of 6 and 7 at concentrations of 2.0 and 4.0 mol%, respectively.

While the main function of some dopants is to behave as densifier agents, others improve the electrical properties by providing valence electrons or by generating potential barriers at the grain boundaries. A homogeneous dispersion of dopants over the entire volume of the varistor is crucial to obtain the same electrical properties in any direction. In the existing literature, it has been reported that there is a strong relationship between the quality of connections between each of the SnO_2 grains and the value of the coefficient α [20,21]. There are three main types of connections: ohmic, non-ohmic, and conductive. In addition to the above, large differences in the value of the potential barriers also affect the electrical conduction, and therefore the value of α. The scope of this work did not consider control over the dopants responsible for improving the electrical properties, thus the quality of the grain boundaries is uncertain. In the varistors obtained by nano-particles, the accumulation of the Co_2SnO_4 phase in the grain boundaries is evident, but this behavior is detrimental to obtaining high values in the α coefficient. In contrast, when micro-particles of Co_3O_4 are used, and the amounts of Co_2SnO_4 are smaller, the value of the α coefficient is increased.

4. Conclusions

SnO_2-based varistors were successfully produce with the use of Co_3O_4 micro and nano-particles. By comparing the systems prepared with micro and nano-particles of Co_3O_4, the densification repeatability attribute was improved using nano-particles. The formation of the spinel phase Co_2SnO_4 was obtained at 16°C lower with the use of nano-particles than with micro-particles. The maximum value of grain size was obtained through the addition of 0.5 and 1.0 mol% of Co_3O_4 nano-particles. The ceramic samples with Co_3O_4 nano-particles exhibit promising electrical properties. In order to confirm this assertion, further research will be performed to improve the non-linear behavior.

Acknowledgments

This study was supported by the National Science and Technology Council of Mexico (CONACYT) under the project Convocatoria Ciencia Básica 2014 (project number 238054).

Martín I. Miranda López is grateful to CONACYT-México for providing a research scholarship.

1. D.R. Clarke, *J. Am. Ceram. Soc.* **82** (1999) 485.
2. Y. Yan, Z. Li, H. Yu, D. Dang, and Z. Liu, *An Online Leakage Current Monitoring System of MOV used in Series Capacitor Compensation*. In 2018 International Conference on Power System Technology (POWERCON). (2018); 3541.
3. G.M.M.M. Lustosa, J.P.d.C. da Costa, L.A. Perazolli, B.D. Stojanovic, and M.A. Zaghete, *J. Am. Ceram. Soc.* **99** (2016) 152.
4. P.R. Bueno, J.A. Varela, and E. Longo, *J. Eur. Ceram. Soc*. **28** (2008) 505.
5. T. Kimura, S. Inada, and T. Yamaguchi, *J. Mater. Sci*. **24** (1989) 220.
6. T.S. Zhang *et al*., *Acta Materialia*. **62** (2014) 81.
7. J.A. Aguilar-Martinez *et al.*, *Rev. Mex. Fis*. **54** (2008) 20.
8. P. Mahmoudi, A. Nemati, and M. Maleki Shahraki, *J. Alloy. Compd.* **770** (2019) 784.
9. N. Yongvanich, K. Niyomtrum, C. Chairatanaset, and T. Srisethkul, *Ceram. Int*. **43** (2017) S280.
10. J.A. Aguilar-Martínez *et al.*, *Ceram. Int*. **42** (2016) 7576.
11. R. Metz, D. Koumeir, J. Morel, J. Pansiot, M. Houabes, and M. Hassanzadeh, *J. Eur. Ceram. Soc*. **28** (2008) 829.
12. M.M. Shahraki, M. Golmohammad, I. Safaee, and M.D. Chermahini, *Ceram. Int*. **44** (2018) 3388.
13. M.G. Masteghin, J.A. Varela, and M.O. Orlandi, *J. Eur. Ceram. Soc*. **37** (2017) 1535.
14. M. Maleki Shahraki, M.A. Bahrevar, and S.M.S. Mirghafourian, *Ceram. Int*. **41** (2015) 6920.
15. S.S. Mali, J.V. Patil, H. Kim, and C.K. Hong, *Nanoscale*. **10** (2018) 8275.
16. A.I. Aparnev, L.I. Afonina, A.V. Loginov, and N.F. Uvarov, *Russ. J. Appl. Chem*. **89** (2016) 212.
17. M.B. Hernández, S. García-Villareal, R.F. Cienfuegos-Pelaes, C. Gómez-Rodríguez, and J.A. Aguilar-Martínez, *J. Alloy. Compd*. **699** (2017) 738.
18. P.N. Plessow and F. Abild-Pedersen, *ACS Catalysis*. **6** (2016) 7098.
19. S.A. Pianaro, P.R. Bueno, E. Longo, and J.A. Varela, *J. Mater. Sci. Lett.* **14** (1995) 692.
20. M.G. Masteghin, R.C. Bertinotti, and M.O. Orlandi, *Ceram. Int*. **43** (2017) 13759.
21. J.S. Vasconcelos *et al.*, *Appl. Phys. Lett*. **89** (2006) 152102.